Fluorinated Benzoselenadiazole-Based Low-Band-Gap Polymers for High Efficiency Inverted Single and Tandem Organic Photovoltaic Cells

ARTICLE *in* MACROMOLECULES · FEBRUARY 2014

Impact Factor: 5.8 · DOI: 10.1021/ma4026493

Macromolecules

Article

pubs.acs.org/Macromolecules

Fluorinated Benzoselenadiazole-Based Low-Band-Gap Polymers for High Efficiency Inverted Single and Tandem Organic Photovoltaic Cells

Ji-Hoon Kim,[†] Seung Ah Shin,[†] Jong Baek Park,[†] Chang Eun Song,[‡] Won Suk Shin,[⊥] Hoichang Yang,[∥] Yongfang Li,[§] and Do-Hoon Hwang*,[†]

[†]Department of Chemistry and Chemistry Institute for Functional Materials, Pusan National University, Busan 609-735, Republic of Korea

[‡]Department of Materials Science and Engineering KAIST, Daejeon 305-701, Republic of Korea

[∥]Department of Advanced Fiber Engineering, Optoelectronic Hybrids Research Center, Inha University, Incheon 402-751, Republic of Korea

[⊥]Korea Research Institute of Chemical Technology, 100 Jang-dong, Yuseong-gu, Daejeon 305-343, Republic of Korea

[§]Beijing National Laboratory for Molecular Sciences and Key Laboratory of Organic Solids, Institute of Chemistry, Chinese Academy of Sciences, Beijing 100190, China

Supporting Information

ABSTRACT: We designed and synthesized two low-band-gap conjugated copolymers with alternating difluorinated benzoselenadiazole (DFDTBSe) and ethylhexyloxy (EH)- or octyldodecyloxy (OD)-substituted benzo[1,2-b:4,5-b′]-dithiophene (BDT) building blocks. PEHBDT-DFDTBSe and PODBDT-DFDTBSe have optical band gap energies of 1.66 and 1.69 eV, respectively, and HOMO energy levels of −5.44 and −5.43 eV, respectively. The different alkyloxy side chains in the polymers affect the molecular packing and ordering in active-layer films blended with [6,6]-phenyl-C_{71} butyric acid methyl ester ($PC_{71}BM$). The PEHBDT-DFDTBSe:$PC_{71}BM$ film comprises predominantly "face-on" crystal structures with short $\pi-\pi$ stacking distances (3.69 Å) while PODBDT-DFDTBSe:$PC_{71}BM$ has mostly "edge-on" structures according to two-dimensional grazing-incidence X-ray diffraction analysis. Bulk heterojunction solar cells were fabricated with an inverted structure of ITO/ethoxylated polyethylenimine/polymer:$PC_{71}BM$/MoO_3/Ag. The device fabricated using the PEHBDT-DFDTBSe:$PC_{71}BM$ active layer shows a maximum power conversion efficiency (PCE) of up to 5.74%, which is the highest value reported for OPVs containing benzoselenadiazole and BDT-derivative polymers. A tandem solar cell was also fabricated using PEHBDT-DFDTBSe:$PC_{71}BM$ and poly(3-hexylthiophene):indene-C_{60}-bisadduct as the top and bottom cell components, respectively; its maximum PCE was 7.15%.

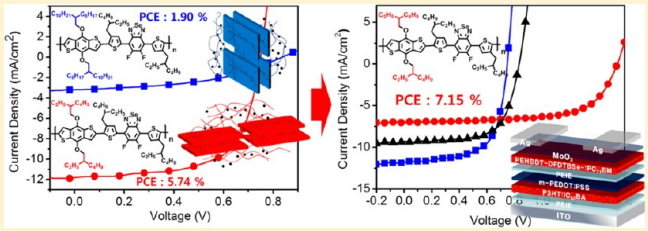

INTRODUCTION

Research into bulk heterojunction (BHJ) organic photovoltaic cells (OPVs) has attracted much attention in both academia and industry because of their potential application in flexible and lightweight solar cells via cost-effective solution processes. Over the past several years, progress on the design and synthesis of p-type electron donor polymers along with the development of novel device architectures and precise morphology control has led to dramatic enhancement of the power conversion efficiency (PCE) of BHJ OPVs. Accordingly, a number of conjugated polymers with PCEs higher than 8% have been reported.[1−5]

Conjugated polymers for high-performance BHJ OPVs should have, at least, the three following features: (1) A low band gap and strong absorption for harvesting sunlight, (2) good energy matching between the frontier orbitals of the polymer donor and fullerene acceptor for efficient charge separation in the photoactive layer, and (3) high charge-carrier mobility of both the donor polymer and acceptor for fast exciton diffusion, charge transport, and efficient charge collection. Donor−acceptor- (D−A-) type conjugated polymers have become the most successful class of p-type semiconductors for BHJ OPVs since they usually have a low band gap and their HOMO and LUMO energy levels can be easily tuned via molecular design.[6−10]

In terms of device geometry, tandem cells, which comprise two subcells stacked in series and contain individual photoactive layers with complementary absorption spectra, have been

Received: December 29, 2013
Revised: February 18, 2014
Published: February 28, 2014

   dx.doi.org/10.1021/ma4026493 | Macromolecules 2014, 47, 1613−1622

Scheme 1. Synthesis and Chemical Structure of DFDTBSe

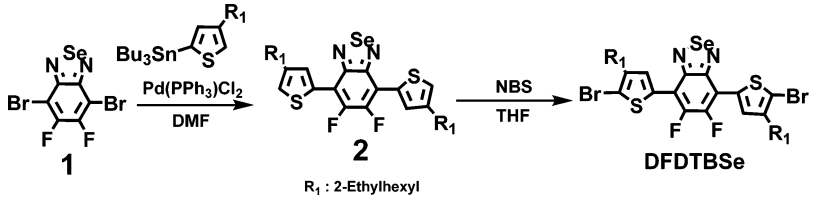

Scheme 2. Syntheses and Chemical Structures of the Polymers

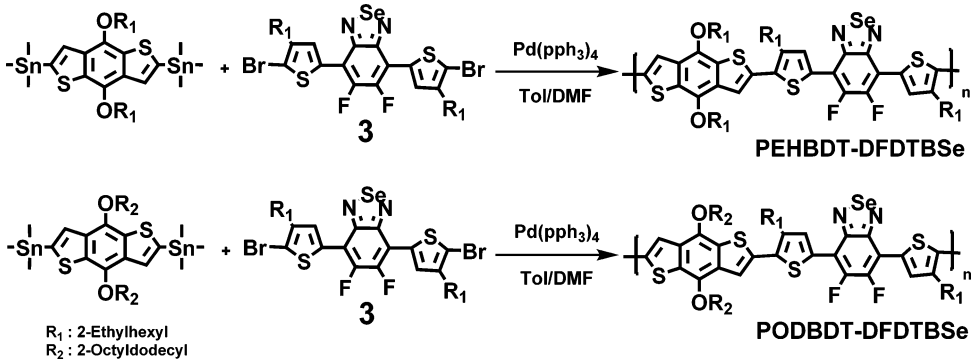

demonstrated to have higher PCEs than classic solar cells. According to the simulated results by Dennler et al., tandem cells should be able to achieve PCEs of up to 15%; recently, PCEs greater than 10% have been reported for both polymer tandem cells and vacuum-processed small-molecule tandem cells.[11−14]

Sulfur-containing heteroaromatic rings have been the most widely used as the electron-donating building blocks for the D−A type low-band gap polymers.[15−22] Recently, heteroaromatic rings containing selenium have attracted much attention as electron-donating building blocks because the polymers absorb in the longer wavelength region of the solar spectrum and have high hole mobility due to strong interchain interactions between Se atoms. Accordingly, benzoselenadiazole (BSe), which is an analogue of the well-known electron acceptor, benzothiadiazole (BT), should impart broader light absorption and higher hole mobility in D−A-type conjugated polymers.[23−28] Tajima and co-workers reported a low-band gap conjugated polymer, i.e., poly[4,8-di(2-octyldodecyloxy)benzo-[1,2-b;3,4-b]-dithiophene-2,6-diyl-*alt*-4,7-dithien-2-yl-2,1,3-benzoselenadiazole-5′,5″-diyl] (PBDT-DTBSe), that exhibits a broad absorption between 300 and 800 nm and has a narrow band gap (∼1.55 eV); the OPV device fabricated using PBDT-DTBSe has a PCE of 5.18%.[24] Li and co-workers reported fluorinated DTBSe-based low-band-gap conjugated polymers, i.e., poly[4,8-di(2-ethylhexylthenyl)benzo[1,2-b;3,4-b]-dithiophene-2,6-diyl-*alt*-4,7-dithien-2-yl-*alt*-4,7-dithien-2-yl-5,6-difuoro-benzo[1,2,5]selenadiazole-5′,5″-diyl] (PBDTBSe), which exhibit a broad absorption between 300 and 750 nm and have a narrow band gap (∼1.66 eV); the OPV device fabricated using PBDTBSe has a PCE of 2.20%.[25]

Recently, we reported dialkoxy-substituted BSe-based low-band-gap polymers with good solubility, broad absorption, and high hole mobility. The OPV device fabricated using the dialkoxy-substituted BSe-based low-band-gap polymers showed a maximum power conversion efficiency of 3.57%.[29] Owing to the electron-withdrawing character of fluorine, fluorinated conjugated polymers usually exhibit low HOMO energy levels and high V_{oc} values in OPVs. We independently reported a low-band-gap conjugated polymer consisting of difluorinated BSe (DFBSe) and 4,8-dioctyldodecyloxybenzo[1,2-*b*;3,4-*b*]-dithiophene (BDT); the OPV device fabricated using PBDT-DFBSe showed a maximum PCE of 1.90%.[30]

Here, we further optimized the structure of PBDT-DFBSe by introducing difluorinated bisthienyl BSe (DFDTBSe) as an electron-accepting part instead of the DFBSe, and also we used different alkyloxy-side chains in BDT unit as electron-donating part to give PEHBDT-DFDTBSe and PODBDT-DFDTBSe as shown in Scheme 1. We investigated the effect of the alkyloxyl side chains on the molecular ordering and optoelectronic properties of the polymer films. The synthesized polymers were characterized by UV−visible absorption, cyclic voltammetry, two-dimensional grazing-incidence X-ray diffraction (2D-GIXD), and hole mobility measurements. The inverted BHJ OPVs fabricated using PEHBDT-DFDTBSe and $PC_{71}BM$ exhibited maximum PCEs of 5.74%, which is the highest value reported for devices fabricated using benzoselenadiazole-containing polymers. Tandem OPVs were also fabricated using PEHBDT-DFDTBSe:$PC_{71}BM$ and P3HT/$IC_{60}BA$ as the top and bottom cell components, respectively. The fabricated tandem cell shows a maximum PCE of 7.15%.

RESULTS AND DISCUSSION

Polymer Synthesis and Characterization. The synthetic routes and chemical structures of the monomers and two polymers are outlined in Schemes 1 and 2, respectively. 4,7-Dibromo-5,6-difluorobenzo[*c*][1,2,5]selenadiazole (**1**) was synthesized according to reported procedures.[28] PEHBDT-DFDTBSe and PODBDT-DFDTBSe were subsequently prepared by Stille-coupling polymerization with DFDTBSe and ethylhexyloxy- or octyldodecyloxy-substituted BDT monomers (i.e., EHBDT or ODBDT) using a $Pd(pph_3)_4$ catalyst. The crude copolymers were purified by successive washing with hot methanol, hexane, and acetone using a Soxhlet extractor. Both copolymers are soluble in common organic solvents, such as chloroform (CF), chlorobenzene (CB), and *o*-dichlorobenzene (*o*-DCB). The average molecular weights and polydisper-

dx.doi.org/10.1021/ma4026493 | *Macromolecules* 2014, 47, 1613−1622

sity indices (PDIs) of the polymers were determined using gel permeation chromatography (GPC) calibrated with polystyrene standards. The number-average molecular weights (M_n) of PEHBDT-DFDTBSe and PODBDT-DFDTBSe were 17 000 and 18 000 g/mol, respectively, with PDIs of 4.12 and 2.17, respectively.

The thermal stability of the copolymers was investigated by thermogravimetric analysis (TGA); PEHBDT-DFDTBSe and PODBDT-DFDTBSe had good thermal stability with decomposition temperatures (5% weight loss) of 398 and 321 °C, respectively (Figure S1). Table 1 summarizes the molecular weights and thermal properties of the synthesized copolymers.

Table 1. Molecular Weights and Thermal Properties of the Synthesized Copolymers

polymer	M_n[a] (g/mol)	M_w[a] (g/mol)	PDI[a]	T_d (°C)[b]
PEHBDT-DFDTBSe	17 000	70 000	4.12	398
PODBDT-DFDTBSe	18 000	39 000	2.17	321

[a]Determined by GPC in chloroform based on polystyrene standards. [b]Decomposition temperature, determined by TGA in nitrogen, based on 5% weight loss.

Optical and Electrochemical Properties. The absorption spectra for PEHBDT-DFDTBSe and PODBDT-DFDTBSe in chloroform solutions and solid films are shown in Figure 1. The

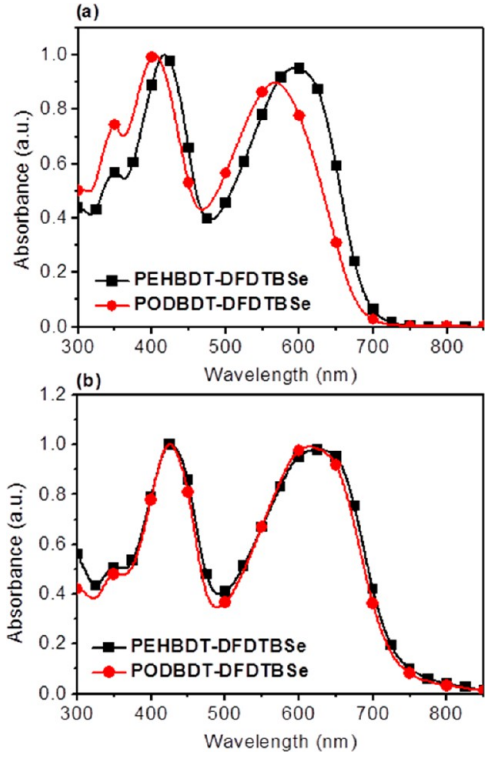

Figure 1. Normalized absorption spectra of PEHBDT-DFDTBSe and PODBDT-DFDTBSe in (a) chloroform solution and (b) thin films.

absorption bands in the range of 350−500 and 500−750 nm are attributed to localized $\pi-\pi^*$ transitions and intermolecular charge transfer (ICT) between the electron-rich BDT units and electron-deficient fluorinated BSe units, respectively.[31] PEHBDT-DFDTBSe showed maximum absorptions at 419 and 597 nm while those of PODBDT-DFDTBSe were at 404 and 567 nm. In comparison, those of the corresponding polymer films moved to longer wavelengths with maximum absorptions at 426 and 627 nm and 426 and 617 nm, respectively. A red shift in the absorption spectra of the polymer films (Figure 1b) from those of the corresponding solutions (Figure 1a) is commonly observed in conjugated polymers due to aggregation of the polymer main chains and enhanced interchain interactions in the solid state. In particular, there are shoulder peaks in the long wavelength region of the PEHBDT-DFDTBSe film, which indicate that ordered structures exist in the polymer films. The optical band gap energies (E_g^{opt}) of the PEHBDT-DFDTBSe and PODBDT-DFDTBSe films were determined to be 1.66 and 1.69 eV, respectively, by measuring their UV−visible absorption onsets. Table 2 summarizes the absorption peak wavelengths (λ_{abs}), absorption edge wavelengths (λ_{edge}), and optical band gaps (E_g^{opt}) of the polymers.

The HOMO and LUMO energy levels of PEHBDT-DFDTBSe and PODBDT-DFDTBSe films were determined using cyclic voltammetry (CV) with a platinum plate as the counter electrode and Ag/Ag^+ as the reference electrode in anhydrous acetonitrile with 0.1 M tetrabutylammonium tetrafluoroborate ($TBABF_4$) at a scan rate of 50 mV/s.[32] Cyclic voltammograms of the polymer films are shown in Figure S2. The reduction potential of $PC_{71}BM$ was also measured by CV at the same conditions. The measured LUMO energy level of $PC_{71}BM$ was −4.00 eV. The cyclic voltammograms of the polymer films and $PC_{71}BM$ solution are shown in the Supporting Information. The HOMO energy values were determined using the following equation: $E_{HOMO} = -e(E_{ox}^{onset} + 4.72)$ eV, where E_{ox}^{onset} is the onset oxidation potential versus Ag/Ag^+. On the basis of the onset values of the oxidation potentials of PEHBDT-DFDTBSe and PODBDT-DFDTBSe (i.e., 0.72 and 0.71 V, respectively), the HOMO energy levels of PEHBDT-DFDTBSe and PODBDT-DFDTBSe were calculated to be −5.44 and −5.43 eV, respectively. The LUMO levels of the polymers were determined by combining the measured HOMO levels and E_g^{opt} values. The LUMO levels of PEHBDT-DFDTBSe and PODBDT-DFDTBSe were measured to be −3.75 and −3.74 eV, respectively. The UV−visible absorption properties, E_g^{opt} values, and HOMO/LUMO energy levels of the polymers are summarized in Table 2.

Film Morphologies and Fabrication of Inverted BHJ OPVs. Inverted OPVs were fabricated using the two polymers and $PC_{71}BM$ with the following configuration: ITO/ethoxylated polyethlyenimine (PEIE)/polymer:$PC_{71}BM$/MoO_3/Ag.[33] The performance of the prepared OPVs was significantly affected by the processing parameters, such as solvent type, blend ratio of the polymer and $PC_{71}BM$, and addition of processing additives. The performances of the fabricated OPV devices were investigated under a variety of conditions. The OPV devices showed the highest short-circuit current density (J_{sc}) and PCE with a polymer/$PC_{71}BM$ blend ratio of 1:2 (Supporting Information). The active layers were spin-coated from different solvents (i.e., CF, CB, and *o*-DCB), and 1,8-diiodooctane (DIO, 3 vol %) was used as a processing additive to optimize the morphology of the active layer. The V_{oc}, J_{sc}, FF, and PCE values of the fabricated devices are summarized in Table 3. Figure 2(a) shows current-density−voltage ($J-V$) curves of the OPVs based on the polymer:$PC_{71}BM$ blends under AM 1.5G illumination (100 mW/cm^2). The best PCEs were obtained when the active layer was processed with chloroform solvent containing 3 vol % DIO.

dx.doi.org/10.1021/ma4026493 | *Macromolecules* 2014, 47, 1613−1622

Table 2. Optical and Electrochemical Properties of the Two Copolymers

polymers	$\lambda_{max,abs}$ (nm) solution[a]	λ_{max} (nm) film[b]	λ_{edge} (nm) film[c]	E_g^{opt} (eV)[d]	HOMO (eV)[e]	LUMO (eV)[e]
PEHBDT-DFDTBSe	419, 597	426, 627	744	1.66	−5.44	−3.78
PODBDT-DFDTBSe	404, 567	426, 617	732	1.69	−5.43	−3.74

[a]Measured in dilute chloroform solution. [b]Measured on quartz plate by polymers cast from chloroform solution. [c]Absorption edge of the thin films. [d]Estimated from the onset wavelength of the absorption spectra: $E_g^{opt} = 1240/\lambda_{edge}$. [e]HOMO = −e($E_{onset}^{ox}$ + 4.70) (eV); LUMO = E_g^{opt} + HOMO (eV).

Table 3. Photovoltaic Properties of the Inverted Single Junction OPVs Containing the Polymers and $PC_{71}BM$ (1:2 w/w) as the Donors and Acceptors, Respectively, under AM 1.5G (100 mW/cm^2) Illumination[a]

polymer	solvent	V_{oc} [V]	J_{sc} [mA/cm^2]	FF	PCE [%]
PEHBDT-DFDTBSe	CF + DIO	0.75	11.82	0.65	5.74
	CB + DIO	0.73	11.93	0.66	5.72
	o-DCB + DIO	0.76	10.42	0.61	4.86
PODBDT-DFDTBSe	CF + DIO	0.84	3.20	0.45	1.22
	CB + DIO	0.77	4.27	0.58	1.90
	o-DCB + DIO	0.75	2.91	0.55	1.20

[a]ITO/PEIE/Polymers:$PC_{71}BM$/MoO_3/Ag configuration.

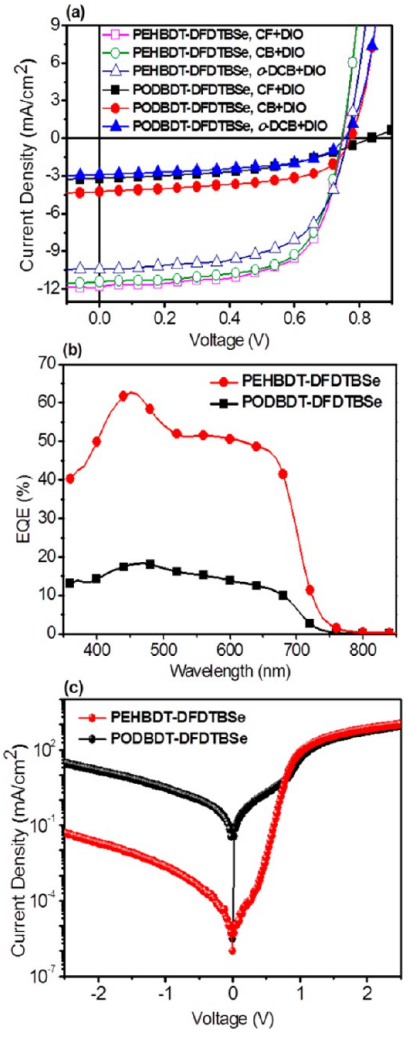

Figure 2. (a) *J*−*V* characteristics of OPVs fabricated from polymer/$PC_{71}BM$ (1:2 w/w, processed with 3 vol % DIO) with different solvents under AM 1.5G illumination (100 mW/cm^2), (b) EQEs of the corresponding devices, and (c) *J*−*V* characteristics of regular single junction OPVs fabricated from polymer/$PC_{71}BM$ (1:2 w/w with DIO) in the dark.

As shown in Figure 2a and Table 3, the regular single-layer inverted OPV devices exhibited maximum PCEs of 5.74 and 1.90% for PEHBDT-DFDTBSe and PODBDT-DFDTBSe, respectively. It is well-known that the V_{oc} is proportional to the energy gap between the HOMO energy level of the donor polymer and LUMO energy level of acceptor. The HOMO energy levels for PEHBDT-DFDTBSe and PODBDT-DFDTBSe measured using CV were very similar; therefore, the two polymers exhibited similar V_{oc} values. The J_{sc} of an OPV is affected by many factors including the absorption of the active layer and charge carrier mobility. Interestingly, the J_{sc} values of the devices fabricated using the two polymers were significantly different. The measured J_{sc} values of the devices fabricated using PEHBDT-DFDTBSe and PODBDT-DFDTBSe were 11.82 and 4.27 mA/cm^2, respectively. The huge difference in the J_{sc} values of the two devices likely originates from the different molecular orientations, charge mobilities, and p−n heterojunction morphologies of the active layers.

Two-dimensional grazing-incidence X-ray diffraction measurements were performed to investigate the crystalline structures of the active layers.[34] Samples were prepared by spin-coating the polymer and blend solutions onto PEIE-coated Si substrates. Figure 3 shows 2D-GIXD images of the pure polymers and polymer:$PC_{71}BM$ (1:2 w/w) blends. The 2D-GIXD pattern of the PEHBDT-DFDTBSe film showed an intense X-ray reflection at Q_z = 0.39 Å^{-1}, which corresponds to the (100) crystal planes of "edge-on" molecules with layer spacing, $d_{(100)}$, of 16.1 Å (Figure 3a). Additionally, a strong X-ray reflection peak corresponding to the (010) crystal planes stacked via intermolecular $\pi-\pi$ interactions was located at Q_z = 1.64 Å^{-1}, which indicates a $d_{(010)}$ of 3.83 Å. Similarly, the 2D-GIXD pattern of the PODBDT-DFDTBSe film showed reflection peaks along the Q_z axis with measured $d_{(100)}$ and $d_{(010)}$ values of 20.9 and 3.78 Å, respectively (Figure 3b).

Interestingly, when the polymer:$PC_{71}BM$ blend films were spun-cast from CF containing 3 vol % DIO, the crystalline structures of these polymers were significantly dependent on the alkyloxy substituents. The 2D-GIXD pattern of the PEHBDT-DFDTBSe:$PC_{71}BM$ (1:2 w/w) film clearly shows enhanced crystallinity and indicates that the polymer chain in the blend film is primarily oriented "face-on" with respect to the substrate (Figures 3, parts c and e). As shown in the out-of-

dx.doi.org/10.1021/ma4026493 | Macromolecules 2014, 47, 1613−1622

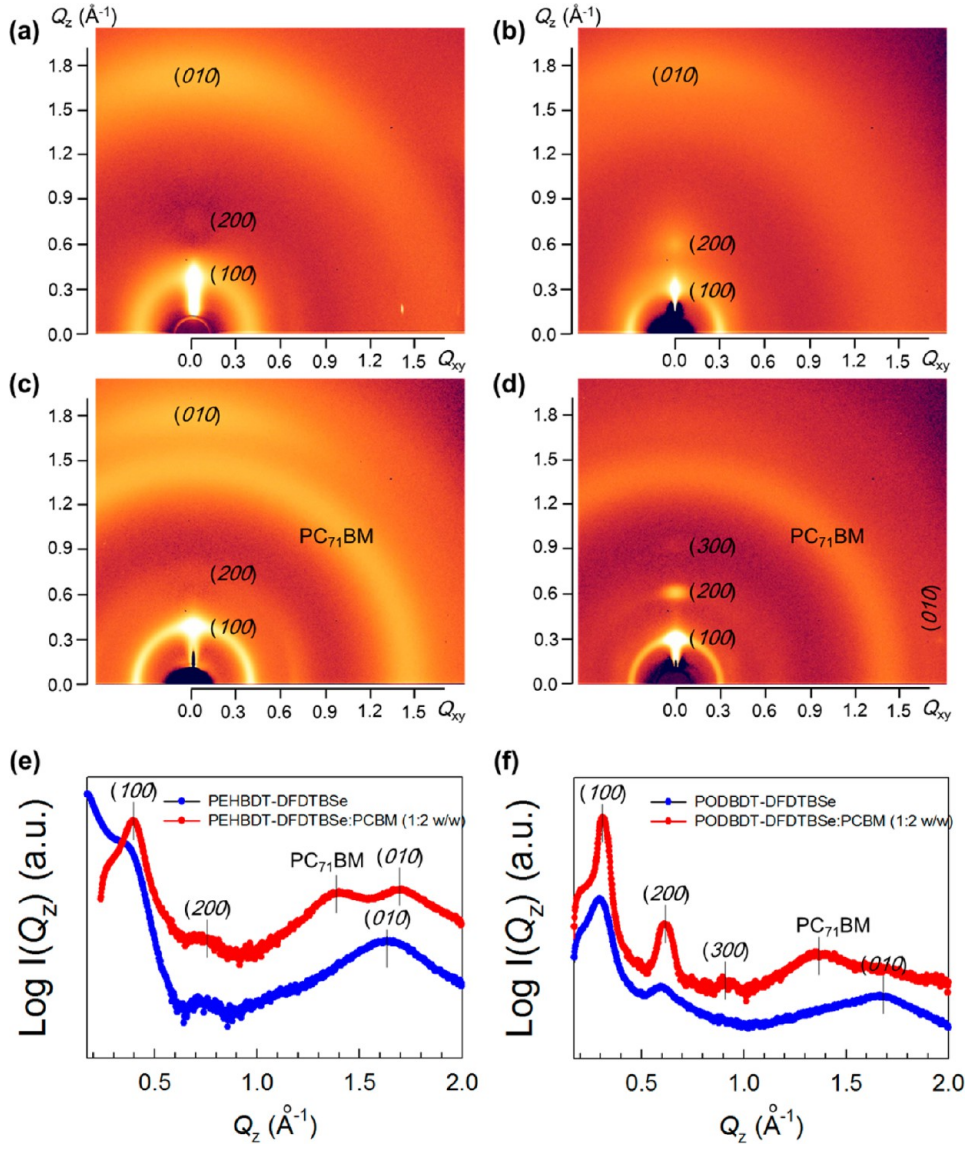

Figure 3. Two-dimensional (2D) grazing-incidence X-ray diffraction (GIXD) pattern of (a, b) pure PEHBDT-DFDTBSe and PODBDT-DFDTBSe and (c, d) PEHBDT-DFDTBSe and PODBDT-DFDTBSe:PC$_{71}$BM (1:2 w/w, with DIO) blend films. (e) Out-of-plane and (f) in-plane slices of the 2D-GIXD spectra.

plane X-ray profile (Figure 3e), an X-ray reflection of the (010) crystal planes in the blend film is present at Q_z = 1.70 Å^{-1} ($d_{(010)}$ = 3.69 Å), which is higher than that of the pure PEHBDT-DFDTBSe film at 1.64 Å^{-1} ($d_{(010)}$ = 3.82 Å). Interestingly, in sharp contrast to that of the PEHBDT-DFDTBSe film, the 2D-GIXD pattern of PODBDT-DFDTBSe:PC$_{71}$BM film showed highly ordered (100) reflections and weak (010) reflections along the Q_z and Q_{xy} axes, respectively, suggesting that the PODBDT-DFDTBSe chains in the blend film are primarily oriented "edge-on" with respect to the substrate (Figures 3, parts d and f). "Face-on" stacking of donor polymers in the active layer is more favorable for charge conduction than "edge-on" stacking. The 2D-XRD analyses of the active layers provide evidence for the origin of the higher J_{sc} values of the OPV devices fabricated using PEHBDT-DFDTBSe:PC$_{71}$BM as compared to those of the devices fabricated using PODBDT-DFDTBSe:PC$_{71}$BM. A simplified schematic morphological model of the two polymer films and two active layers generated from the 2D-GIXD results are illustrated in Figure 4.

To elucidate the vertical charge carrier mobility in OPV devices, we fabricated hole-only devices to determine the space charge limited current (SCLC). The hole-only device was fabricated with structures of ITO/PEDOT:PSS(30 nm)/pure PEHBDT-DFDTBSe or PEHBDT-DFDTBSe and PEHBDT-DFDTBSe:PC$_{71}$BM (1:2 w/w) or PODBDT-DFDTBSe:PC$_{71}$BM (1:2 w/w)/Au; the mobilities were calculated using the Mott-Gurney equation.[35] The hole mobilities of the PEHBDT-DFDTBSe and PODBDT-DFDTBSe films were similar at 1.00 × 10^{-5} and 1.52 × 10^{-5} cm^2 V^{-1} s^{-1}, respectively, at an electric field of 500 (V cm^{-1})$^{1/2}$, as shown in Figure 5. Interestingly, the hole mobilities of the polymers changed significantly after blending with PC$_{71}$BM acceptor. The measured hole mobilities of PEHBDT-DFDTBSe:PC$_{71}$BM (1:2 w/w) and PODBDT-DFDTBSe:PC$_{71}$BM (1:2 w/w) were 2.26 × 10^{-5} and 3.78 × 10^{-6} cm^2 V^{-1} s^{-1}, respectively. According to the 2D-GIXD

dx.doi.org/10.1021/ma4026493 | Macromolecules 2014, 47, 1613−1622

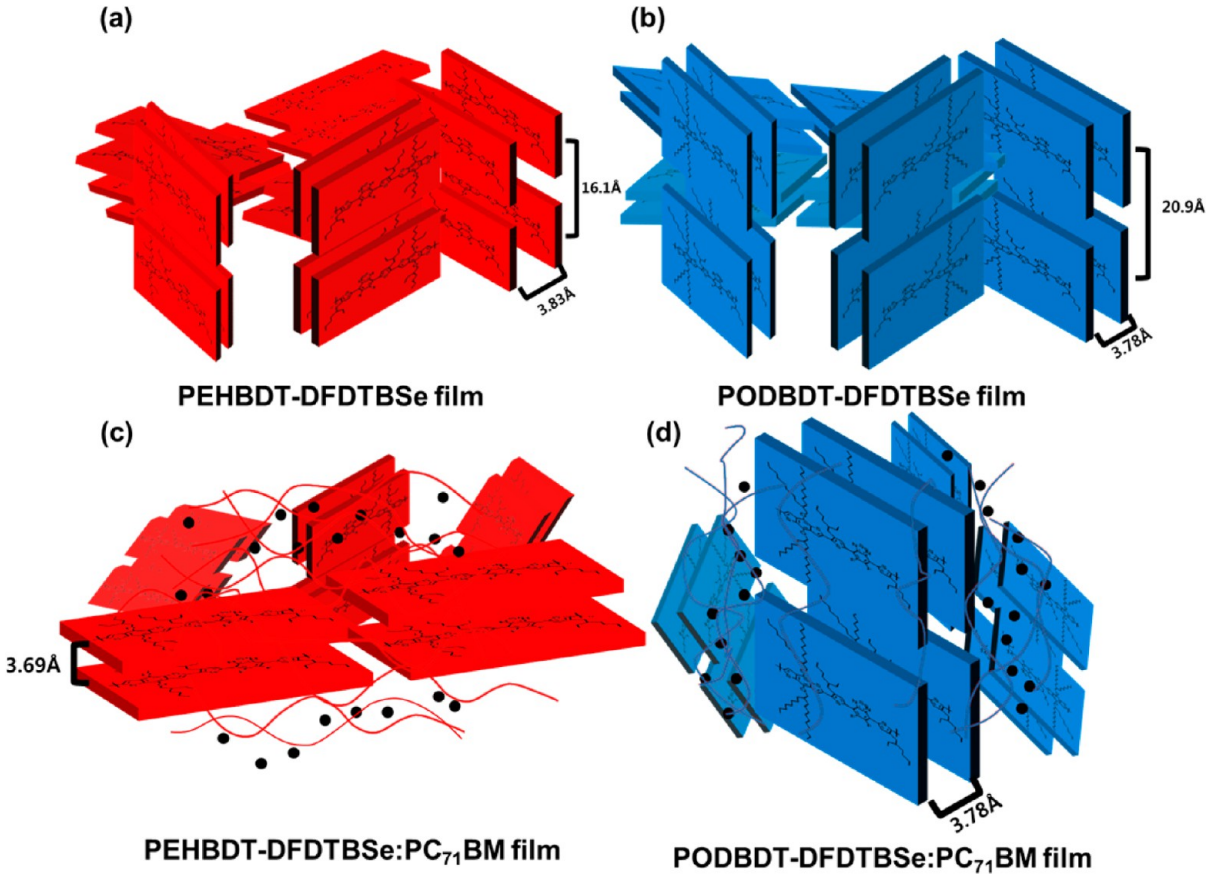

Figure 4. Schematic morphological models (simplified) of (a, b) pure PEHBDT-DFDTBSe and PODBDT-DFDTBSe and (c, d) PEHBDT-DFDTBSe and PODBDT-DFDTBSe:$PC_{71}BM$ (1:2 w/w, with DIO) blend films.

analysis, PEHBDT-DFDTBSe:$PC_{71}BM$ showed "face-on" orientation with a shorter $\pi-\pi$ stacking distance of 3.69 Å while PODBDT-DFDTBSe:$PC_{71}BM$ exhibited "edge-on" crystal orientation. We could expect that the "face-on" oriented PEHBDT-DFDTBSe:$PC_{71}BM$ film would have higher hole mobility than the "edge-on" oriented PODBDT-DFDTBSe:$PC_{71}BM$ film in the vertically structured OPV cells. Therefore, the measured SCLC mobilities are consistent with the crystal structures of the two active layers. The higher hole mobility of PEHBDT-DFDTBSe:$PC_{71}BM$ are also consistent with its higher J_{sc} and *FF* values than those of PODBDT-DFDTBSe:$PC_{71}BM$ device. The characteristics of the fabricated SCLC results are summarized in Table 4.

Figure 2b shows the external quantum efficiency (EQE) curves of OPVs fabricated under the same optimized conditions. The PEHBDT-DFDTBSe device showed higher photoconversion efficiency than the PODBDT-DFDTBSe device. The J_{sc} values calculated by integrating the EQE curves with an AM 1.5G reference spectrum are within 5% deviation from the corresponding J_{sc} values obtained from the $J-V$ curves. The spectral responses from the OPV devices showed that photons within the spectral range of 350−700 nm contributed significantly to the EQE. The maximum EQEs were 63% at 450 nm and 20% at 470 nm for the devices fabricated using PEHBDT-DFDTBSe and PODBDT-DFDTBSe, respectively.

A well-organized p−n heterojunction morphology of the active layer is important for efficient charge dissociation and transport. Transmission electron microscopy (TEM) images were obtained to investigate the morphology of the active layer films with copolymer:$PC_{71}BM$ films (1:2 w/w) processed with 3 vol % DIO. In the TEM images (Figure 6), the dark and light regions correspond to $PC_{71}BM$ and polymer domains, respectively. The PEHBDT-DFDTBSe:$PC_{71}BM$ (1:2 w/w, 3 vol % DIO) blend film contains uniform and well-organized bicontinuous networks, which indicate good miscibility between PEHBDT-DFDTBSe and $PC_{71}BM$. In contrast, the PODBDT-DFDTBSe:$PC_{71}BM$ (1:2 w/w, 3 vol % DIO) blend film exhibited much larger p−n junction domains. These large-scale domains are not favorable for efficient exciton dissociation, leading to relatively low J_{sc} values. The TEM results also support the higher J_{sc} of the device fabricated using PEHBDT-DFDTBSe than that of the device containing PODBDT-DFDTBSe.

Inverted Tandem Photovoltaic Cells Performance. The versatile photovoltaic applications of PEHBDT-DFDTBSe are demonstrated by its use in solution-processed inverted tandem photovoltaic cells. A tandem photovoltaic cell enables effective harvesting of a broader portion of the solar spectrum and makes more efficient use of the photonic energy than a single junction structure. Tandem OPVs with inverted configurations were fabricated using PEHBDT-DFDTBSe:$PC_{71}BM$ as the top cell component. Poly(3-hexylthiophene) (P3HT) and indene-C_{60}-bisadduct ($IC_{60}BA$) were used as the bottom cell donor and acceptor materials, respectively. The structure of the fabricated tandem cell was ITO/PEIE/P3HT:$IC_{60}BA$ (150 nm)/PEDOT:PSS/PEIE/PEHBDT-DFDTBSe:$PC_{71}BM$(80 nm)/MoO_3/Ag. Figure 7

dx.doi.org/10.1021/ma4026493 | *Macromolecules* 2014, 47, 1613−1622

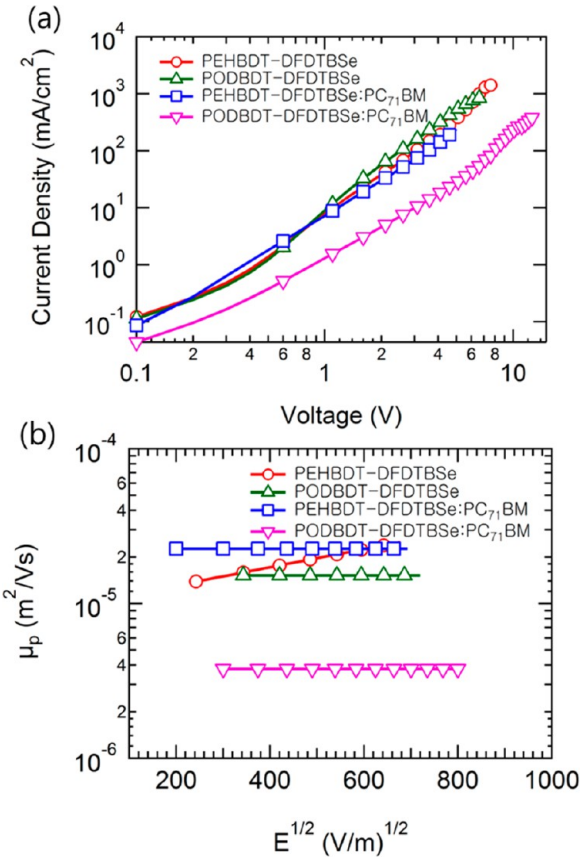

Figure 5. (a) $J-V$ characteristics of the hole-only devices and (b) field-dependent hole mobilities of pure polymer and polymer:$PC_{71}BM$ blend films calculated from the hole-only devices by fitting $J-V$ curves in the SCLC regime.

Table 4. Calculated Hole Mobilities of the Polymers and Polymer/$PC_{71}BM$ (1:2 w/w) System at Optimized Conditions Using the SCLC Method

active layer	solvent	thickness (nm)	μ_h[a] ($cm^2\ V^{-1}\ s^{-1}$)
PEHBDT-DFDTBSe	CF	100	1.00×10^{-5}
PEHBDT-DFDTBSe:$PC_{71}BM$	CF + DIO	70	2.26×10^{-5}
PODBDT-DFDTBSe	CF	100	1.52×10^{-5}
PODBDT-DFDTBSe:$PC_{71}BM$	CF + DIO	70	3.78×10^{-6}

[a]The hole-only devices with structure of ITO/PEDOT:PSS/active layer/MoO_3/Au.

shows the device structure and UV−visible absorption spectra of P3HT and PEHBDT-DFDTBSe in the solid state. The overlap of the absorption spectra of PEHBDT-DFDTBSe and P3HT is not significant, and the materials complementarily cover the solar spectrum from 350 to 750 nm, indicating a good match for the tandem cell. The organic tandem photovoltaic cells fabricated for this study have an inverted architecture with a conducting polymer layer of PEDOT:PSS coated with PEIE as the charge recombination layer, as shown in Figure 7.[9,33] The $J-V$ characteristics of the tandem cells and performance parameters are shown in Figure 8. The optimized tandem cells exhibit maximum PCEs as high as 7.15%. The devices have a V_{oc} of 1.55 V, which is equal to the sum of the V_{oc}s of the single bottom and top cells, and a J_{sc} of 7.03 mA/cm^2 and FF of greater than 0.66 were achieved. The tandem cell shows a higher V_{oc} than those of the individual cells while the FF is close

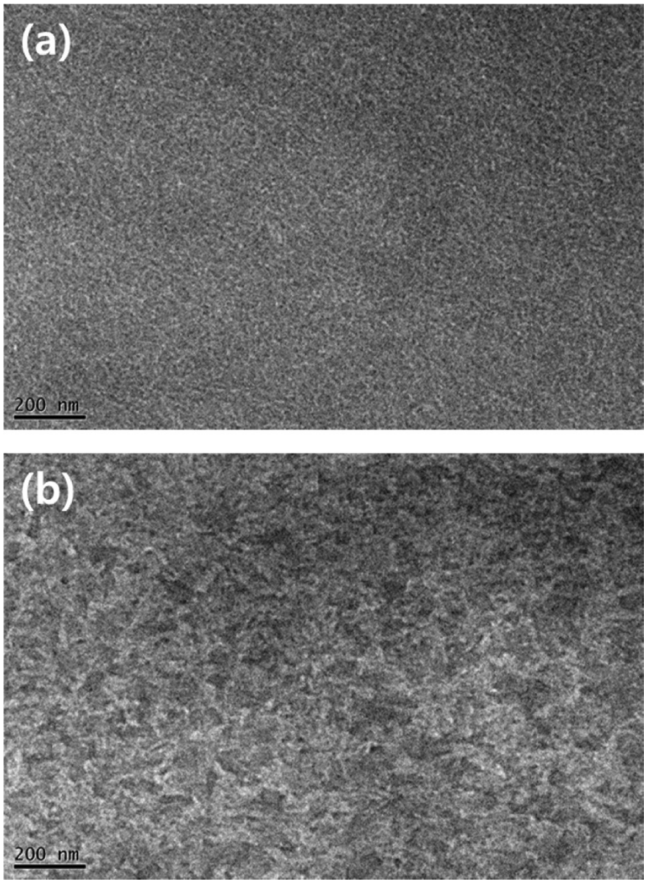

Figure 6. TEM images of (a) PEHBDT-DFDTBSe:$PC_{71}BM$ blends (1:2 w/w) and (b) PODBDT-DFDTBSe:$PC_{71}BM$ blends (1:2 w/w) cast from chlorobenzene with 3 vol % DIO.

to the average of those of the individual cells, which is in accordance with the results from other tandem cells.[36,37] The photovoltaic performance of the inverted tandem device is summarized in Table 5.

CONCLUSIONS

In conclusion, we successfully synthesized and characterized PEHBDT-DFDTBSe and PODBDT-DFDTBSe by Stille cross-coupling polymerization. The different alkyloxy side chains in the polymers affect the molecular ordering in the $PC_{71}BM$-blended active layer films. The PEHBDT-DFDTBSe:$PC_{71}BM$ film comprises a primarily "face-on" crystal structure with a short intermolecular $\pi-\pi$ stacking distance while PODBDT-DFDTBSe:$PC_{71}BM$ primarily comprises an "edge-on" structure. These 2D-GIXD results are consistent with the higher SCLC hole mobility of the PEHBDT-DFDTBSe:$PC_{71}BM$ film than that of the PODBDT-DFDTBSe:$PC_{71}BM$ film. The inverted bulk heterojunction OPVs fabricated using PEHBDT-DFDTBSe:$PC_{71}BM$ exhibit PCEs of 5.74%, and the tandem OPVs fabricated using PEHBDT-DFDTBSe:$PC_{71}BM$ as the top cell and P3HT:$IC_{60}BA$ as the bottom cell show a maximum PCE of 7.15%.

EXPERIMENTAL SECTION

Materials. All starting organic compounds were purchased from Aldrich, Alfa Aesar, or TCI Korea and used without further purification. Bis(triphenylphosphine)palladium(II)chloride and tetrakis(triphenylphosphine)palladium(0) were purchased from Strem. Indene-C_{60} bisadduct ($IC_{60}BA$) and [6,6]-phenyl C_{71}-butyric

dx.doi.org/10.1021/ma4026493 | Macromolecules 2014, 47, 1613−1622

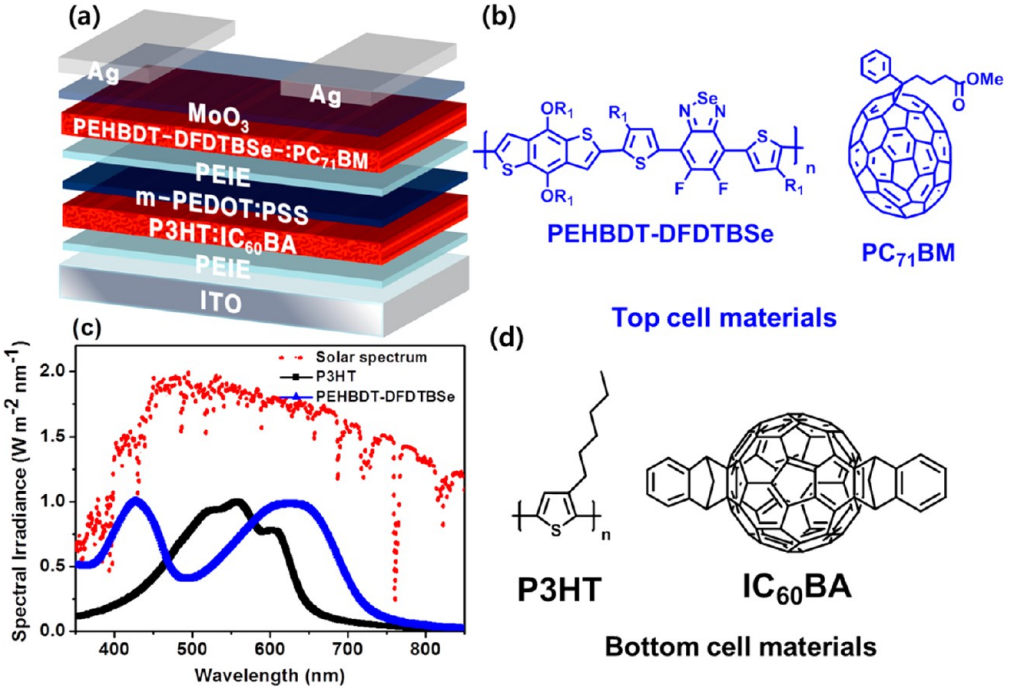

Figure 7. Inverted tandem photovoltaic device. (a) Device structure of the inverted tandem photovoltaic device. (b) Chemical structures of P_3HT, $IC_{60}BA$, $PC_{71}BM$, and PEHBDT-DFDTBSe. (c) UV−visible spectra of the P_3HT of the bottom cell, PEHBDT-DFDTBSe of the top cell, and the solar spectrum.

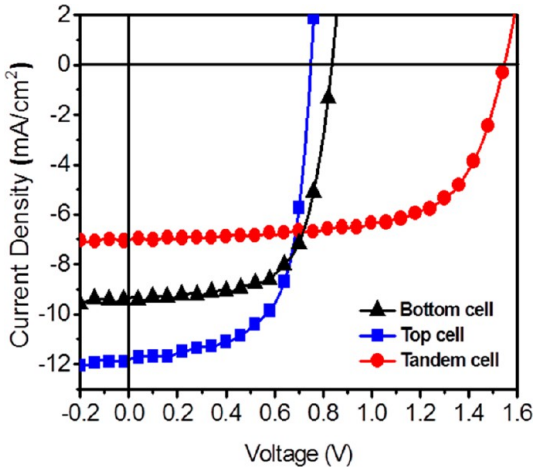

Figure 8. Current density−voltage characteristics of the single-junction bottom cell, single-junction top cell, and inverted tandem cell under AM1.5G illumination (100 mW/cm^2).

acid methyl ester ($PC_{71}BM$) were purchased from EM-Index. Poly(3-hexylthiophene) (P3HT) was purchased from Rieke Metals. Solvents were dried and purified by fractional distillation over sodium/benzophenone and handled in a moisture-free atmosphere. Column chromatography was performed using silica gel (Merck, Kieselgel 60 63−200 MYM SC). 2,6-Bis(trimethyltin)-4,8-diethylhexyloxybenzo-[1,2-*b*;3,4-*b*]dithiophene, 2,6-bis(trimethyltin)-4,8-dioctyldodecyloxybenzo[1,2-*b*;3,4-*b*]dithiophene, and 4,7-dibromo-5,6-difluoro[2,1,3]benzoselenadiazole (DFBSe) were synthesized similarly to the methods described in previous reports.[30,38]

Measurements. ^1H and ^{13}C NMR spectra were recorded using a Varian Mercury Plus 300 MHz spectrometer, and the chemical shifts were recorded in units of ppm versus the shift of chloroform as the internal standard. The absorption spectra were measured using a JASCO JP/V-570 instrument. The molecular weights of the polymers were determined by gel permeation chromatography (GPC) analysis relative to a polystyrene standard using a Waters high-pressure GPC assembly (model M590). Thermal analyses were performed on a Mettler Toledo TGA/SDTA 851^e under a nitrogen atmosphere with a heating and cooling rate of 10 °C/min. Cyclic voltammetry (CV) was performed on a CH Instruments Electrochemical Analyzer. The CV measurements were carried out in acetonitrile solutions containing 0.1 M tetrabutylammonium tetrafluoroborate ($TBABF_4$) as the supporting electrolyte, with a $Ag/AgNO_3$ reference electrode, platinum wire counter electrode, and platinum working electrode.

Two-Dimensional (2D) Grazing-Incidence X-ray Diffraction (GIXD) Experiments. 2D-GIXD measurements were performed on the 3C beamline at the Pohang Accelerator Laboratory (South Korea). X-rays with a wavelength of 1.1651 Å (10.6408 keV) were used. The incidence angle (0.13°) was chosen to allow for complete penetration of the X-rays into the polymer film.

Table 5. Characteristics of PEHBDT-DFDTBSe-Based Inverted Tandem OPVs (Inverted Single and Inverted Tandem) under AM 1.5G (100 mW/cm^2) Illumination

inverted	cell	active layer	weight ratio [w/w]	thickness [nm]	V_{oc} [V]	J_{sc} [mA/cm^2]	FF	PCE [%]
tandem	bottom[a]	P3HT:$IC_{60}BA$	1:1	150	0.83	9.33	0.66	5.15
cells	top[b]	PEHBDT-DFDTBSe: $PC_{70}BM$	1:2	80	0.75	11.82	0.65	5.74
	tandem[c]	–	–	–	1.55	7.03	0.66	7.15

[a]ITO/PEIE/P3HT:$IC_{60}BA$/MoO_3/Ag configuration. [b]ITO/PEIE/PEHBDT-DFDTBSe:$PC_{71}BM$/MoO_3/Ag configuration. [c]ITO/PEIE/P3HT:$IC_{60}BA$/PEDOT:PSS/PEIE/PEHBDT-DFDTBSe:$PC_{71}BM$/MoO_3/Ag configuration.

dx.doi.org/10.1021/ma4026493 | *Macromolecules* 2014, 47, 1613−1622

Fabrication of Inverted Photovoltaic Devices. Inverted BHJ OPVs devices with ITO/PEIE (ethoxylated polyethlyenimine)/polymer:$PC_{71}BM$/MoO_3/Ag structures were fabricated. The precleaned ITO substrates were treated with UV-ozone. The PEIE solution was spin-coated onto the ITO substrates at a speed of 5000 rpm for 1 min at an acceleration of 1000 rpm/s and annealed at 120 °C for 10 min on a hot plate in ambient air. The thickness of PEIE was estimated to be 10 nm. The substrates were then transferred into a N_2-filled glovebox. The polymer:$PC_{71}BM$ (97% chlorobenzene/3% DIO mixture) active layer was prepared by spin coating at a speed of 1000 rpm for 30 s. The device was solvent-annealed for 1 h at the ambient temperature in the glovebox. The device fabrication was completed by thermal evaporation of 10 nm MoO_3 and 100 nm Ag as the anode *in vacuo* at a base pressure of 3×10^{-6} Torr. The effective area of the device was 0.09 cm^2.

Inverted Tandem Cells. The device architecture of the tandem photovoltaic cell is shown in Figure 6. The precleaned ITO substrates were treated with UV-ozone. The PEIE solution was spin-coated onto ITO substrates at a speed of 5000 rpm for 1 min at an acceleration of 1000 rpm/s and annealed at 120 °C for 10 min on a hot plate in ambient air. The thickness of PEIE was estimated to be 10 nm. The substrates were then transferred into a N_2-filled glovebox. The P3HT:$IC_{60}BA$ (1.0:1.0 weight ratio in *o*-dichlorobenzene) bottom layer was prepared by spin coating at a speed of 800 rpm for 30 s. P3HT was purchased from Rieke Metals. $IC_{60}BA$ was purchased from EM-Index. The P3HT:$IC_{60}BA$ device was solvent-annealed for 1 h at the ambient temperature in the glovebox. To directly coat the hydrophilic PEDOT:PSS onto the hydrophobic active layer, a 30 nm thick PEDOT:PSS layer (Clevios P VP AI4083) with Triton X-100 (1 wt %) (laboratory grade, Sigma-Aldrich) surfactant was spin-casted. PEDOT:PSS was then coated with PEIE using the same conditions described previously. The top PTTBDT-FTT:$PC_{71}BM$ (1:1.5 weight ratio in chlorobenzene with 3 vol % DIO) active layer was deposited by spin-coating at 1000 rpm for 20 s. The thickness of PTTBDT-FTT:$PC_{71}BM$ was estimated to be 80 nm. The device fabrication was completed by thermal evaporation of 10 nm MoO_3 and 100 nm Ag as the anode *in vacuo* at a base pressure of 3×10^{-6} Torr. The effective area of the device was 0.09 cm^2.

Measurements of the OPV Devices. The thickness of the active layer was measured using a KLA Tencor Alpha-step IQ surface profilometer. The current-density−voltage ($J-V$) characteristics of the polymer photovoltaic cells were determined by illuminating the cells with simulated solar light (AM 1.5G) at an intensity of 100 mW/cm^2 using an Oriel 1000 W solar simulator. Electronic data were recorded using a Keithley 236 source-measure unit, and all characterizations were carried out under ambient conditions. The illumination intensity was calibrated using a standard Si photodiode detector from PV Measurements Inc., which was calibrated at the National Renewable Energy Laboratory (NREL).

Mobility Measurement. The hole mobilities of the active layer were determined by applying the space charge limited current (SCLC) model to the $J-V$ measurements of the devices. The hole-only devices of the polymers were fabricated on top of a prepatterned ITO substrate. After cleaning the ITO with aqueous detergent, deionized water, acetone, and 2-propanol, UV-ozone treatment was applied for 15 min. PEDOT:PSS (Clevios P VP AI4083) was spin-coated from an aqueous dispersion phase to a layer 30 nm thick. The coated substrate was then baked at 120 °C for 60 min. After baking, a solution of the copolymer in chloroform was spin-cast on top of the PEDOT:PSS layer to a thickness of ∼100 nm, and the samples were dried for 6 h at room temperature under vacuum conditions. The device fabrication was completed by thermal evaporation of 10 nm MoO_3 and 100 nm Al as the anode *in vacuo* at a base pressure of 3×10^{-6} Torr. A similar way was employed to measure the hole only mobility of the polymer:PC71BM blend through the space charge-limited current (SCLC) method with a device structure of ITO/PEDOT:PSS/polymer:PC71BM/MoO_3/Au. The hole mobilities were calculated from the space charge limited current (SCLC) using the following equation:

$$J_{SCLC} = (9/8)\varepsilon_r\varepsilon_0\mu(V^2/L^3)$$

where J is the current density, ε_r is the dielectric constant of the polymers, ε_o is the permittivity of the vacuum, μ is the hole mobility, L is the film thickness of the blend films, $V = V_{appl} - V_{bi}$, V_{appl} is the applied potential, and V_{bi} is the built-in voltage which results from the difference in the work function of the anode and the cathode.

Syntheses of Monomers and Polymers. *Synthesis of 5,6-Difluoro-4,7-bis(4-(2-ethylhexyl)-2-thienyl)-2,1,3-benzoselenadiazole (2).* Compound **1** (1.00 g, 2.65 mmol) and 5-(2-ethylhexyl)-2-(tributylstannyl)thiophene (3.86 g, 7.96 mmol) were dissolved in dry DMF (30 mL) and the reaction mixture was heated at reflux for 24 h under a N_2 atmosphere. The mixture was extracted twice with ethyl acetate and the organic phase was subsequently dried over anhydrous Na_2SO_4. Recrystallization from methanol gave the title compound as a dark red solid (yield: 0.80 g, 50%). ^{1}H NMR (300 MHz, $CDCl_3$, δ): 7.97 (s, 2H), 7.19 (s, 2H), 2.65 (d, 4H), 1.64−1.63 (m, 2H), 1.37−1.25 (m, 16H), 0.96−0.89 (t, 12H).^{13}C NMR (75 MHz, $CDCl_3$, δ): 155.4, 146.7, 138.6, 137.1, 127.5, 126.7, 99.3, 41.8, 36.5, 32.2, 29.6, 25.3, 14.1, 11.9.

Synthesis of 4,7-Bis(5-bromo-4-(2-ethylhexyl)-2-thienyl)-5,6-difluoro-2,1,3-benzoselenadiazole (DFDTBSe). *N*-Bromosuccinimide (NBS; 0.54 g, 3.02 mmol) was added in one portion to a solution of compound **2** (0.80 g, 1.32 mmol) in glacial acetic acid (50 mL) and chloroform (50 mL). The mixture was stirred at room temperature in the dark for 24 h. The mixture was then extracted twice with dichloromethane, and the organic phase was subsequently dried over anhydrous Na_2SO_4. Recrystallization from methanol gave the title compound as a dark red solid (yield: 0.80 g, 79%).^{1}H NMR (300 MHz, $CDCl_3$, δ): 7.81 (s, 2H), 2.60 (d,4H), 1.69 (m, 2H), 1.40−1.32 (m, 16H), 0.89 (m, 12H). ^{13}C NMR (75 MHz, $CDCl_3$, δ): 155.4, 146.7, 142.3, 139.7, 129.0, 115.0, 99.3, 41.1, 32.7, 32.2, 29.6, 25.3, 23.0, 14.1, 11.9.

General Polymerization Procedure. All copolymers were synthesized using Stille cross-coupling. A solution of the monomers and tetrakis(triphenylphosphine)palladium in anhydrous toluene (8 mL) and dimethylformamide (DMF; 1 mL) was stirred at 120 °C for 2 d. Excess 2-bromothiophene and tripropyl(thiophen-2-yl)stannane end-cappers dissolved in anhydrous toluene (1 mL) were added and the mixture was stirred for an additional 12 h. The mixtures were then cooled to ∼50 °C and poured into methanol (200 mL) with vigorous stirring. The resulting polymer fibers were collected by filtration and further purified by washing for 2 day in a Soxhlet apparatus using acetone to remove any remnant oligomers and catalyst residues followed by silica gel column chromatography using chloroform as the eluent. The resulting polymers were soluble in common organic solvents.

Synthesis of PEHBDT-DFDTBSe. This polymerization was performed using a reaction mixture of 2,6-bis(trimethyltin)-4,8-diethylhexyloxybenzo[1,2-*b*;3,4-*b*]dithiophene (300 mg, 0.36 mmol), 4,7-bis(5-bromo-4-(2-ethylhexyl)-2-thienyl)-5,6-difluoro-2,1,3-benzoselenadiazole (297 mg, 1.0 equiv), tetrakis(triphenylphosphine) palladium (14 mg, 3.0 μmol), toluene (8 mL), and DMF (1 mL). ^{1}H NMR (300 MHz, $CDCl_3$, δ): 7.89 (s. 2H), 7.58 (s, 2H), 4.05 (s, 4H), 2.83 (s, 4H), 1.80 (s, 4H), 1.32 (m, 32H), 0.92 (m, 24H).

Synthesis of PODBDT-DFDTBSe. This polymerization was performed using a reaction mixture of 2,6-bis(trimethyltin)-4,8-dioctyldodecyloxybenzo[1,2-*b*;3,4-*b*]dithiophene (230 mg, 0.21 mmol), 4,7-bis(5-bromo-4-(2-ethylhexyl)-2-thienyl)-5,6-difluoro-2,1,3-benzoselenadiazole (159 mg, 1.0 equiv), tetrakis-(triphenylphosphine)palladium (7 mg, 3.0 μmol), toluene (8 mL), and DMF (1 mL). ^{1}H NMR (300 MHz, $CDCl_3$, δ): 8.01 (s, 2H), 7.55 (s, 2H), 4.19 (s, 4H), 2.90 (s, 4H), 1.82 (s, 4H), 1.22 (m, 72H), 0.89 (m, 24H).

dx.doi.org/10.1021/ma4026493 | *Macromolecules* 2014, 47, 1613−1622

■ ASSOCIATED CONTENT

Supporting Information

TGA, DSC, CV curves, ^{1}H NMR spectra, and OPV data. This material is available free of charge via the Internet at http://pubs.acs.org.

■ AUTHOR INFORMATION

Corresponding Author

*(D.-H.H.) E-mail: dohoonhwang@pusan.ac.kr.

Notes

The authors declare no competing financial interest.

■ ACKNOWLEDGMENTS

This work was supported by a grant (No. 2012055225) from the Center for Advanced Soft Electronics under the Global Frontier Research Program of the Ministry of Education, Science and Technology, Korea, and a New and Renewable Energy Program of the Korea Institute of Energy Technology Evaluation and Planning (KETEP) funded by the Korean government Ministry of Trade, Industry & Energy (20113010010030), and a National Research Foundation (NRF) grant funded by the Korean government (MEST) through GCRC SOP (No. 2011-0030668).

■ REFERENCES

(1) McCullough, R. D.; Lowe, R. D. *J. Chem. Soc., Chem. Commun.* **1992**, *1*, 70.

(2) Sariciftci, N. S.; Smilowitz, L.; Heeger, A. J.; Wudl, F. *Science* **1992**, *258*, 1474.

(3) Xin, H.; Subramaniyan, S.; Kwon, T.-W.; Shoaee, S.; Durrant, J. R.; Jenekhe, S. A. *Chem. Mater.* **2012**, *24*, 1995.

(4) (a) Krebs, F. C.; Gevorgyan, S. A.; Alstrup, J. *J. Mater. Chem.* **2009**, *19*, 5442. (b) Helgesen, M.; Søndergaard, R.; Krebs, F. C. *J. Mater. Chem.* **2010**, *20*, 36.

(5) Park, J. K.; Jo, J.; Seo, J. H.; Moon, J. S.; Park, Y. D.; Lee, K.; Heeger, A. J.; Bazan, G. C. *Adv. Mater.* **2011**, *23*, 2430.

(6) Sista, S.; Z. Hong, R.; Chen, L. M.; Yang, Y. *Energy Environ. Sci.* **2011**, *4*, 1606.

(7) Ameri, T.; Dennler, G.; Lungenschmied, C.; Brabec, C. J. *Energy Environ. Sci.* **2009**, *2*, 347.

(8) Kim, J. Y.; Lee, K.; Coates, N. E.; Moses, D.; Nguyen, T. Q.; Dante, M.; Heeger, A. J. *Science* **2007**, *317*, 222.

(9) Zhou, Y. H.; Fuentes-Hernandez, C.; Shim, J. W.; Khan, T. M.; Kippelen, B. *Energy Environ. Sci.* **2012**, *5*, 9827.

(10) Gevaerts, V. S.; Furlan, A.; Wienk, M. M.; Turbiez, M.; Janssen, R. A. J. *Adv. Mater.* **2012**, *24*, 2130.

(11) Dennler, G.; Scharber, M. C.; Ameri, T.; Denk, P.; Forberich, K.; Waldauf, C.; Brabec, C. J. *Adv. Mater.* **2008**, *20*, 579.

(12) Dou, L.; Chang, W.-H.; Gao, J.; Chen, C.-C.; You, J.; Yang, Y. *Adv. Mater.* **2013**, *25*, 825.

(13) Kim, J.-H.; Song, C. E.; Kim, H. U.; Grimsdale, A. C.; Moon, S. J.; Shin, W. S.; Choi, S. K.; Hwang, D.-H. *Chem. Mater.* **2013**, *25*, 2722.

(14) Kim, J.-H.; Song, C. E.; Kang, I. N.; Shin, W. S.; Hwang, D.-H. *Chem. Commun.* **2013**, *49*, 3248.

(15) Blouin, N.; Michaud, A.; Gendron, D.; Wakim, S.; Blair, E.; Neagu-Plesu, R.; Belletete, M.; Durocher, G.; Tao, Y.; Leclerc, M. *J. Am. Chem. Soc.* **2008**, *130*, 732.

(16) Zhang, M.; Gu, Y.; Guo, X.; Liu, F.; Zhang, S.; Huo, L.; Russell, T. P.; Hou, J. *Adv. Mater.* **2013**, *25*, 4944.

(17) Huang, Y.; Liu, F.; Guo, X.; Zhang, J.; Han, C. C.; Russell, P. T.; Hou, J. *Adv. Energy Mater.* **2013**, *3*, 930.

(18) Park, S. H.; Roy, A.; Beaupre, S.; Cho, S.; Coates, N.; Moon, J. S.; Moses, D.; Leclerc, M.; Lee, K.; Heeger, A. J. *Nat. Photonics* **2009**, *3*, 297.

(19) Zhou, E.; Wei, Q.; Yamakawa, S.; Zhang, Y.; Tajima, K.; Yang, C.; Hashimoto, K. *Macromolecules* **2010**, *43*, 821.

(20) Zhou, E.; Cong, J.; Hashimoto, K.; Tajima, K. *Energy Environ. Sci.* **2012**, *5*, 9756.

(21) Zhou, E.; Hashimoto, K.; Tajima, K. *Polymer* **2013**, *54*, 6501.

(22) Dou, L.; Chen, C.-C.; Yoshimura, K.; Ohya, K.; Chang, W.-H.; Gao, J.; Liu, Y.; Richard, E.; Yang, Y. *Macromolecules* **2013**, *46*, 3384.

(23) Tang, W.; Chen, W.; Zou, Y.; Liu, B.; Zhong, H.; Pan, C. *J. Appl. Polym. Sci.* **2013**, DOI: 10.1002/APP.38586.

(24) Zhou, E.; Cong, J.; Hashimoto, K.; Tajima, K. *Macromolecules* **2013**, *46*, 763.

(25) Shen, P.; Bin, H.; Zhang, Y.; Li, T. *Polym. Chem.* **2014**, *5*, 567–577.

(26) Zhao, W.; Cai, W.; Xu, R.; Yang, W.; Gong, X.; Wu, H.; Cao, Y. *Polymer* **2010**, *51*, 3196.

(27) Hou, J.; Chen, T. L.; Zhang, S.; Chen, H. Y.; Yang, Y. *J. Phys. Chem. C* **2009**, *113*, 1601.

(28) Hou, J.; Park, M. H.; Zhang, S.; Yao, Y.; Chen, L. M.; Li, J. H.; Yang, Y. *Macromolecules* **2008**, *41*, 6012.

(29) Shin, S. A.; Park, J. B.; Kim, J. H.; Hwang, D. H. *Synth. Met.* **2013**, *172*, 54.

(30) Shin, S. A.; Kim, J. H.; Park, J. B.; Kang, I. N.; Park, M. J.; Hwang, D. H. *Macromol. Chem. Phys.* **2013**, *214*, 1780.

(31) Shen, P.; Bin, H.; Zhang, Y.; Li, Y. *Polym. Chem.* **2014**, *5*, 567.

(32) Li, Y.; Xu, B.; Li, H.; Cheng, W.; Xue, L.; Chen, F.; Lu, H.; Tian, W. *J. Phys. Chem. C* **2011**, *115*, 2386.

(33) Zhou, Y. H.; Fuentes-Hernandez, C.; Shim, J.; Meyer, J.; Giordano, A. J.; Li, H.; Winget, P.; Papadopoulos, T.; Cheun, H.; Kim, J.; Fenoll, M.; Dindar, A.; Haske, W.; Najafabadi, E.; Khan, T. M.; Sojoudi, H.; Barlow, S.; Graham, S.; Brédas, J.-L.; Marder, S. R.; Kahn, A.; Kippelen, B. *Science* **2012**, *336*, 327.

(34) Chen, M. S.; Niskala, J. R.; Unruh, D. A.; Chu, C. K.; Lee, O. P.; Fréchet, J. M. J. *Chem. Mater.* **2013**, *25*, 4088.

(35) Cho, H.-H.; Kang, T. E.; Kim, K.-H.; Kang, H.; Kim, H. J.; Kim, B. J. *Macromolecules* **2012**, *45*, 6415.

(36) Jo, J.; Pouliot, J.-R.; Wynands, D.; Collins, S. D.; Kim, J. Y.; Nguyen, T. L.; Woo, H. Y.; Sun, Y.; Leclerc, M.; Heeger, A. J. *Adv. Mater.* **2013**, *25*, 4783.

(37) You, J.; Chen, C.-C.; Hong, Z.; Yoshimura, K.; Ohya, K.; Xu, R.; Ye, S.; Gao, J.; Li, G.; Yang, Y. *Adv. Mater.* **2013**, *25*, 3973.

(38) Kim, J.-H.; Kim, H. U.; Song, C. U.; Shin, W. S.; Lee, J.-K.; Kang, I.-N.; Lee, J.-K.; Hwang, D.-H. *Sol. Energy Mater. Sol. Cells* **2013**, *108*, 113.